Translational Oncology 14 (2021) 101005

Contents lists available at ScienceDirect

Translational Oncology

journal homepage: www.elsevier.com/locate/tranon

Photodynamic therapy exploiting the anti-tumor activity of mannose-conjugated chlorin e6 reduced M2-like tumor-associated macrophages

Tatsuki Soyama[a], Akira Sakuragi[a], Daisuke Oishi[a], Yuka Kimura[a], Hiromasa Aoki[a], Akihiro Nomoto[b], Shigenobu Yano[c], Hirotada Nishie[d], Hiromi Kataoka[d], Mineyoshi Aoyama[a,*]

[a] Department of Pathobiology, Nagoya City University Graduate School of Pharmaceutical Sciences, 3-1 Tanabe-dori, Mizuho-ku, Nagoya 467-8603, Japan
[b] Department of Applied Chemistry, Graduate School of Engineering, Osaka Prefecture University, 1-1 Gakuen-cho, Naka-ku, Sakai, Osaka 599-8531, Japan
[c] KYOUSEI Science Center for Life and Nature, Nara Women's University, Kitauoya-Higashimachi, Nara 630-8506, Japan
[d] Department of Gastroenterology and Metabolism, Nagoya City University Graduate School of Medical Sciences, 1 Kawasumi, Mizuho-cho, Nagoya 467-8601, Japan

ARTICLE INFO

Keywords:
Tumor-associated macrophage
Tumor microenvironment
Tumor immunity
Photodynamic therapy
Mannose-conjugated chlorin e6

ABSTRACT

M2-like tumor-associated macrophages (M2-TAMs) in cancer tissues are intimately involved in cancer immunosuppression in addition to growth, invasion, angiogenesis, and metastasis. Hence, considerable attention has been focused on cancer immunotherapies targeting M2-TAMs. However, systemic therapies inhibit TAMs as well as other macrophages important for normal immune responses throughout the body. To stimulate tumor immunity with fewer side effects, we targeted M2-TAMs using photodynamic therapy (PDT), which damages cells via a nontoxic photosensitizer with harmless laser irradiation. We synthesized a light-sensitive compound, mannose-conjugated chlorin e6 (M-chlorin e6), which targets mannose receptors highly expressed on M2-TAMs. M-chlorin e6 accumulated more in tumor tissue than normal skin tissue of syngeneic model mice and was more rapidly excreted than the second-generation photosensitizer talaporfin sodium. Furthermore, M-chlorin e6 PDT significantly reduced the volume and weight of tumor tissue. Flow cytometric analysis revealed that M-chlorin e6 PDT decreased the proportion of M2-TAMs and increased that of anti-tumor macrophages, M1-like TAMs. M-chlorin e6 PDT also directly damaged and killed cancer cells *in vitro*. Our data indicate that M-chlorin e6 is a promising new therapeutic agent for cancer PDT.

Introduction

Malignant tumors reside in a niche called the tumor microenvironment (TME), which facilitates the growth and survival of cancer cells. The TME is composed of a variety of cells, including fibroblasts, vascular endothelial cells, myofibroblasts, and immune cells. Tumor-associated macrophages (TAMs) are a class of immune cells present in high numbers in tumor tissues, where they mediate tumorigenesis, tumor angiogenesis, tumor immunosuppression, and metastasis [1–4]. Three TAM phenotypes have been described: inflammatory M1-like TAMs (M1-TAMs), which express CD80 or CD86; anti-inflammatory M2-like TAMs (M2-TAMs), which express CD206 [5]; and non-polarized M0-like TAMs (M0-TAMs) [6]. M1-TAMs play important roles in innate host defense and exert anti-tumor effects by producing reactive oxygen species (ROS) and pro-inflammatory cytokines such as IL-1β and TNF-α. M1-TAMs are thus considered anti-tumor macrophages [5]. M2-TAMs, by contrast, are crucial for humoral immunity, wound healing, and tissue remodeling. M2-TAMs, which produce anti-inflammatory cytokines such as IL-10 and TGF-β, promote tumor growth and development. Various cytokines derived from M2-TAMs suppress the function of helper T cells and cytotoxic T lymphocytes (CTLs), which play a major role in tumor immunity. These cytokines can also induce regulatory T cells (Tregs), which exhibit immunosuppressive functions by directly inhibiting CTLs and secreting immunosuppressive factors. Therefore, M2-TAMs are considered pro-tumor macrophages [7]. M0-TAMs are defined as macrophages that have just infiltrated into tumor tissues but have not yet polarized to M1-TAMs or M2-TAMs [6]. Circulating macrophages and monocytes infiltrate tumors and polarize into M2-TAMs following exposure to humoral factors released by cancer cells and other cells in the TME [8]. Recent evidence suggests that the presence of M2-TAMs is strongly associated with poor prognosis of some cancers [9,10]. Hence, considerable attention has been focused on the development of cancer immunotherapies targeting M2-TAMs [11]. However, in addition to inhibiting TAMs, these therapies also inhibit macrophages that play important roles in normal processes throughout the body, such as tissue remodeling and

* Corresponding author.
E-mail address: aomine@phar.nagoya-cu.ac.jp (M. Aoyama).

https://doi.org/10.1016/j.tranon.2020.101005
Received 22 December 2020; Accepted 26 December 2020

immune responses. Therefore, M2-TAM–targeting therapies carry a risk of inducing immunodeficiency [12,13].

Photodynamic therapy (PDT) is a cancer treatment approach that kills target cells using a harmless visible laser and nontoxic photosensitizer [14]. When light-sensitive substances are exposed to a specific wavelength of the laser, they become energized and enter an excited state. Upon returning to the ground state, they release ROS, leading to apoptosis of target cells. This mechanism ensures that only laser-irradiated tumor sites are damaged. Hence, PDT is expected to become a less invasive, site-selective approach for treating cancers and a variety of other diseases. In Japan, both first-generation PDT using porfimer sodium (also known as Photofrin) and excimer dye laser irradiation at 630 nm and second-generation PDT using talaporfin sodium (also known as Laserphyrin) and diode laser irradiation at 664 nm have been approved for clinical use. However, porfimer sodium PDT has some drawbacks, such as a high frequency of skin phototoxicity and a requirement to avoid direct sunlight for a long period (~4 to 6 weeks). Talaporfin sodium, by contrast, has a short clearance time and exhibits low skin toxicity, with a shorter period of avoiding direct sunlight (~2 weeks) [14,15]. In addition, talaporfin sodium PDT enables the treatment of deeper lesions because the diode laser has a longer wavelength than the excimer dye laser used in porfimer sodium PDT. However, the tumor selectivity of talaporfin sodium is poor [16]. Therefore, we developed a third-generation photosensitizer, glucose-conjugated chlorin e6 (G-chlorin e6) [17,18]. Due to the Warburg effect and expression of GLUT1, G-chlorin e6 is highly selective for cancer cells, which consume more glucose than normal cells. Furthermore, G-chlorin e6 is more rapidly excreted from the body and exerts a strong anti-tumor effect.

During our research regarding sugar-conjugated photosensitizers, we also generated a new photosensitizer, mannose-conjugated chlorin e6 (M-chlorin e6), which is readily excreted from the body. M-chlorin e6 can thus be targeted to M2-TAMs, which highly express mannose receptors (CD206). Cancer cells also take up M-chlorin e6, as mannose is taken up via GLUT1 expressed on cancer cells. In this study, we assessed the effect of M-chlorin e6 PDT on tumor growth and TAM polarization using syngeneic tumor model mice and cultured cells.

Materials and methods

Photosensitizers

M-chlorin e6 (methyl(7*S*,8*S*)-18-ethyl-5-(2-methoxy-2-oxoethyl)-7-(3-methoxy-3-oxopropyl)-2,8,12,17-tetramethyl-13-(1-(3-(((2*S*,3*S*,4*S*,5*S*,6*R*)-3,4,5-trihydroxy-6-(hydroxymethyl)tetrahydro-2*H*-pyran-2-yl)thio)propoxy)ethyl)-7*H*,8*H*-porphyrin-3-carboxylate) and G-chlorin e6 (methyl(7*S*,8*S*)-18-ethyl-5-(2-methoxy-2-oxoethyl)-7-(3-methoxy-3-oxopropyl)-2,8,12,17-tetramethyl-13-(1-(3-(((2*S*,3*R*,4*S*,5*S*,6*R*)-3,4,5-trihydroxy-6-(hydroxymethyl)tetrahydro-2*H*-pyran-2-yl)thio)propoxy)ethyl)-7*H*,8*H*-porphyrin-3-carboxylate) were synthesized and provided by the laboratory of Osaka Prefecture University (Osaka, Japan) [17,18]. M-chlorin e6 was synthesized as described below. 1-Thio-β-D-tetraacetylmannose and 3-(3-bromopropoxy) chlorin-e6-TME were prepared according to methods described in the literature [19–21]. Et_3N (63.5 μL) was added to a stirred solution of 3-(3-bromopropoxy) chlorin-e6-TME (276 mg, 0.078 mmol) in CH_2Cl_2 under a N_2 atmosphere. To the mixture cooled at 0 °C, a solution of 1-thio-β-D-tetraacetylmannose (3.2 equiv.) in CH_2Cl_2 was added dropwise. After stirring for 3 h at room temperature under a N_2 atmosphere, the mixture was transferred to a separating funnel, CH_2Cl_2 and water were added, and the organic layer was separated. The aqueous layer was washed with brine, dried over sodium sulfate, and then evaporated to dryness. The residue was purified by column chromatography (CH_2Cl_2/AcOEt, 1:2) to give acetylated β-M-Ce6. Deprotection was carried out according to ordinary methods. NaOMe/MeOH suspension (10 equiv.) was added to acetylated β-M-Ce6 (0.152 mmol) in dried MeOH under a N_2 atmosphere. After stirring for 5 h at room temperature, the solution was then quenched with AcOH (100 μL), and the mixture was evaporated to dryness. The residue was purified by column chromatography (CH_2Cl_2/AcOEt, 10:1) to give β-M-Ce6. ^{1}H-NMR (400 MHz, $CDCl_3$): $\delta = 9.78$ (d, $J = 13.2$ Hz, 1H), 9.67 (d, $J = 5.2$ Hz, 1H), 8.69 (d, $J = 2.4$ Hz, 1H), 5.85–5.86 (m, 1H), 5.20-5.40 (m, 4H), 4.35–4.50 (m, 2H), 4.20 (s, 3H), 3.85–3.65 (m, 6H), 3.54–3.60 (m, 11H), 3.40–3.50 (m, 2H), 3.42 (s, 3H), 3.29 (s, 3H), 2.90–3.20 (m, 2H), 2.30–2.80 (m, 7H), 2.20–2.05 (m, 3H), 1.65–1.80 (m, 8H) -1.55 (s, 2H). MALDI-TOF-MS: ($C_{46}H_{60}N_4O_{12}S$) calcd. 892.39; found. 892.37. Talaporfin sodium ((+)-tetrasodium (2S,3S)-18-carboxylato-20-[N-(S)-1,2-dicarboxylatoethyl]carbamoylmethyl-13-ethyl-3,7,12,17-tetramethyl-8-vinylchlorin-2-propanoate) was purchased from Meiji Seika Pharma (Tokyo, Japan).

Cell culture

CT26 mouse colon cancer cells and HCT116 human colon cancer cells were purchased from the American Type Culture Collection (Manassas, VA, USA). Cells were cultured at 37 °C in a 5% CO_2, 95% air environment. CT26 cells were grown in low-glucose (1000 mg/L) Dulbecco's modified Eagle's medium (Wako, Osaka, Japan) supplemented with 10% fetal bovine serum, 100 U/mL penicillin, and 100 μg/mL streptomycin.

Animals and tumor models

The present study was approved by the Animal Care and Use Committee of Nagoya City University Graduate School of Pharmaceutical Sciences. All experiments were performed in accordance with institutional and U.S. National Institutes of Health guidelines for the care and use of laboratory animals. Female mice (BALB/cCrSlc) age 4–6 weeks were purchased from Japan SLC (Shizuoka, Japan). Mice were allowed to acclimatize for 1 week in the animal facility before any interventions were initiated. Syngeneic tumor model mice were established by inoculating 2.0×10^6 CT26 cells subcutaneously under the right flank.

In vivo photodynamic diagnosis (PDD)

After the tumor inoculated into each mouse reached approximately 100 mm^3, a solution containing M-chlorin e6, G-chlorin e6, or talaporfin sodium was injected via the tail vein at a dose of 6.25 μmol/kg. Measurements of both the tumor and normal (flank side opposite the tumor) areas were started immediately after intravenous drug injection and averaged 0.5, 1, 2, 3, 4, 5, and 6 h after injection. PDD experiments were performed using a violet semiconductor laser system (VLD-M1/ver.3.0sp) for fluorescence analysis and research. Tumor tissues were laser-irradiated at 405 nm, and the returning spontaneous fluorescence intensity (505 nm)/red fluorescence intensity (655 nm) ratio was determined for each drug. The mice were then euthanized by cervical dislocation.

In vivo PDT

When inoculated tumors reached approximately 100 mm^3, mice were injected intravenously with M-chlorin e6 at a dose of 6.25 μmol/kg. At 30 min after injection, tumors were irradiated with 660-nm LED light at a dose of 30 J/cm^2 (intensity: 49 mW/cm^2) using a LEDR-660DL (Opto Code, Tokyo, Japan).

Measurements of tumor volume and weight

M-chlorin e6 PDT was performed as described above. Tumors were measured using a ruler on days 0, 3, 7, 10, and 14 after LED irradiation, and tumor size was calculated using the following formula: long diameter × short diameter × short diameter/2. On day 14, the mice were euthanized, and the tumors were removed and weighed.

Table 1
RT-qPCR primer sequences.

Gene	Forward primer (5′→3′)	Reverse primer (5′→3′)
iNOS	GCAGAGATTGGAGGCCTTGTG	GGGTTGTTGCTGAACTTCCAGTC
IL-6	CAACGATGATGCACTTGCAGA	CTCCAGGTAGCTATGGTACTCCAGA
TNF-a	CCACCACGCTCTTCTGTCTAC	AGGGTCTGGGCCATAGAACT
IL-1β	TCCAGGATGAGGACATGAGCAC	GAACGTCACACACCAGCAGGTTA
arginase1	AACACGGCAGTGGCTTTAACC	GGTTTTCATGTGGCGCATTC
TGF-β1	GAACCAAGGAGACGGAATACAG	CCATGAGGAGCAGGAAGG
IL-10	GGTTGCCAAGCCTTATCGGA	ACCTGCTCCACTGCCTTGCT

Flow cytometric analysis

M-chlorin e6 PDT was performed as described above. Mice were euthanized by cervical dislocation on day 2 after LED irradiation. The tumors were removed and treated with 10% collagenase (Wako), shredded using a gentleMACS™ Dissociator (Miltenyi Biotec, Bergisch Gladbach, Germany), and passed through a 70-μm filter. Next, 1.0×10^6 cells were mixed with 1 μL of Fc-block/100 μL of stain buffer (BD Biosciences, San Jose, CA) and left on ice for 10 min. Subsequently, 1 μL of fluorescent antibody (CD11b-APC [BD Biosciences], CD206-BV421 [Biolegend, San Diego, CA], CD80-PE [BD Biosciences], CD86-PE-Cy7 [BD Biosciences], CD45-PE-Vio®770 [Miltenyi Biotec], CD3-FITC [Miltenyi Biotec], CD8a-APC-H7 [BD PharMingen, San Diego, CA], CD127-APC [BD PharMingen], CD25-PE [BD Biosciences], or CD4-BV421 [Biolegend]) diluted with 100 μL of stain buffer was added and left on ice for 30 min. The cells were then washed with 500 μL of phosphate-buffered saline (PBS) and suspended in 500 μL of stain buffer. Next, 5 μL of 7-AAD (BD Biosciences) was added to prepare a sampling solution, which was analyzed on a BD FACSVerse™ (BD Biosciences).

Cell sorting

M-chlorin e6 PDT was performed according to the method described above. The sampling solution was adjusted according to the above method, and $CD11b^+$ $7\text{-}AAD^-$ cells ($\sim 3 \times 10^5$) were isolated on a BD FACSAria™ (BD Biosciences).

RNA extraction, reverse transcription, and real-time PCR

The expression of selected genes (iNOS, IL-6, TNF-α, IL-1β, arginase, TGF-β, IL-10, and 18S ribosomal RNA) was analyzed by reverse transcription–real-time PCR (RT-qPCR). Total RNA was isolated from $CD11b^+$ cells using RNAiso plus (Takara Bio, Otsu, Japan) in accordance with the manufacturer's instructions. Reverse transcription was performed using PrimeScript RT Master Mix (Takara Bio), and the resulting cDNAs were subjected to PCR-based amplification. Real-time PCR was performed using Go Taq (Promega Corp., Madison, WI, USA) in a total reaction volume of 12.5 μL containing: 2.5 μL RT product, 0.5 μL forward primer (10 μM), 0.5 μL reverse primer (10 μM), 6.25 μL Go Taq qPCR Master Mix, and 2.75 μL nuclease-free H_2O. Amplification was performed at 95 °C for 2 min, followed by amplification for 40 cycles at 95 °C for 15 s and 55 °C for 1 min using a Thermal Cycler Dice Real-Time System (Takara Bio). Relative target gene transcript levels were normalized to endogenous transcript levels of a housekeeping gene (18S ribosomal RNA) after confirming that the cDNAs from different genes were amplified with the same efficiency. The primer pairs used in this study are listed in Table 1.

In vitro PDT

CT26 cells were seeded into 96-well plates at 5×10^3 cells/well and incubated for 24 h. The cells were then incubated with M-chlorin e6 or G-chlorin e6 for 24 h, washed once in PBS, covered with PBS, and irradiated with 660-nm LED light at a dose of 16 J/cm^2 (intensity: 49 mW/cm^2) using a LEDR-660DL (Opto Code).

Cell viability assay

Cell viability was determined using a WST-8 cell proliferation assay (Cell Counting Kit-8, Dojindo Laboratories, Kumamoto, Japan) in accordance with the manufacturer's instructions. Cells were incubated for 24 h after PDT and then incubated with CCK-8 solution for 1 h, after which the absorbance at 450 nm was measured using an iMark™ Microplate Absorbance Reader (Bio-Rad, Hercules, CA, USA). The plotted data were fit to a four-parameter logistic curve (using Image J function, curve fitting), and IC_{50} values for M-chlorin e6 were calculated.

Statistical analyses

All statistical analyses were performed using EZR (Saitama Medical Center, Jichi Medical University, Saitama, Japan), a graphical user interface for R. Specifically, EZR is a modified version of R Commander designed to add functions frequently used in biostatistics [22]. Two-tailed non-paired Student's *t*-tests were used for comparisons between two groups. One-way analysis of variance followed by Tukey's multiple comparison test were used for multiple comparisons. Two-way repeated measures analysis of variance was used for comparisons of tumor size measured over prolonged periods. Data are presented as the mean ± standard error (SE). A p value of <0.05 was considered statistically significant.

Results

M-chlorin e6 is more rapidly excreted than talaporfin sodium and has a higher accumulation rate in tumors

To target TME M2-TAMs and cancer cells that highly express CD206 on the cell membrane, we generated M-chlorin e6 (Fig. 1A). Using *in vivo* PDD, the accumulation of M-chlorin e6 at tumor sites was compared with that of other photosensitizers, such as talaporfin sodium and G-chlorin e6. Talaporfin sodium did not accumulate at the tumor sites, whereas M-chlorin e6, as well as G-chlorin e6, showed higher accumulation at tumor sites than in normal skin tissue (Fig. 1B). Furthermore, although complete drug excretion was not observed with talaporfin sodium, G-chlorin e6 and M-chlorin e6 were almost completely excreted from the tissues by 6 h after drug administration (Fig. 1B).

M-chlorin e6 PDT inhibits tumor growth

To confirm the treatment effect of M-chlorin e6 PDT, we prepared syngeneic tumor model mice by subcutaneously injecting BALB/c mice with CT26 cells. When the tumors grew to a certain extent, we injected the mice with M-chlorin e6 and irradiated the tumors. After M-chlorin e6 PDT, we monitored tumor growth for 2 weeks (Fig. 2A). Tumor volume was significantly reduced in the M-chlorin e6 PDT group compared with other groups (Fig. 2B and C). We also confirmed that tumor weight was significantly reduced in the M-chlorin e6 PDT group compared with other groups (Fig. 2D).

M-chlorin e6 PDT selectively damages M2-TAMs

Next, we determined the proportion of M2-TAMs in the TME using flow cytometric analyses. Syngeneic tumor model mice were treated with M-chlorin e6 PDT and the tumors were excised for analysis 2 days later. The proportion of TAMs ($CD11b^+$) among all tumor tissue cells in the M-chlorin e6 PDT group was equivalent to that in the control group (Fig. 3A and B). The proportion of M0-TAMs, which are defined as $CD11b^+$, $CD80^-$ or $CD86^-$, $CD206^-$ cells in the present study, was increased in the M-chlorin e6 PDT group compared to the control group (Fig. 3A and C). Furthermore, the proportion of M1-TAMs ($CD11b^+$, $CD80^+$ or $CD86^+$, $CD206^-$) was increased in the PDT group compared

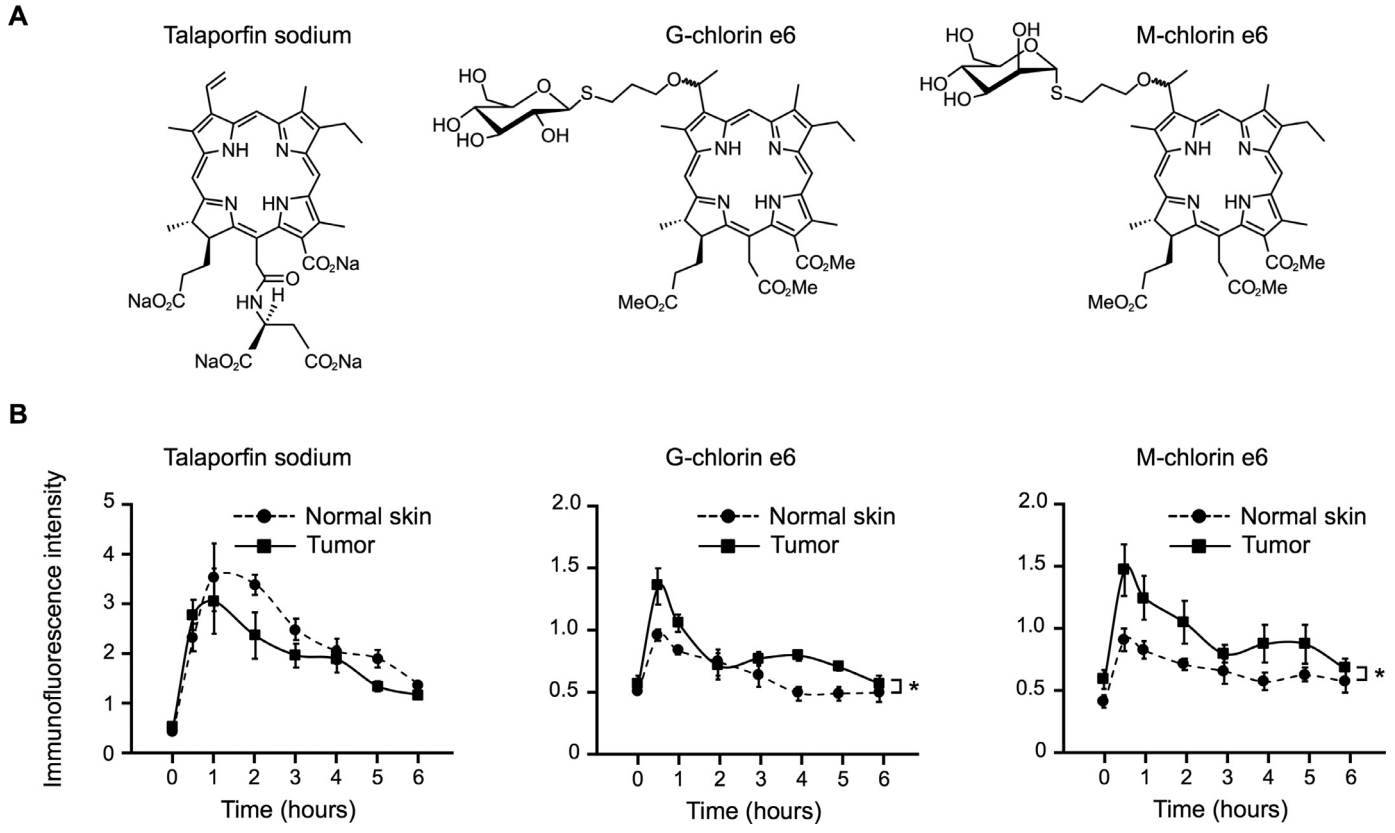

Fig. 1. Analyses of M-chlorin e6 accumulation and excretion.
(A) Chemical structures of talaporfin sodium, G-chlorin e6, and M-chlorin e6.
(B) Accumulation and excretion of talaporfin sodium, G-chlorin e6, and M-chlorin e6 were analyzed by PDD experiments for 6 h. Data are presented as mean ± SE ($n = 4$; $^{*}p < 0.05$; two-way repeated measures analysis of variance).

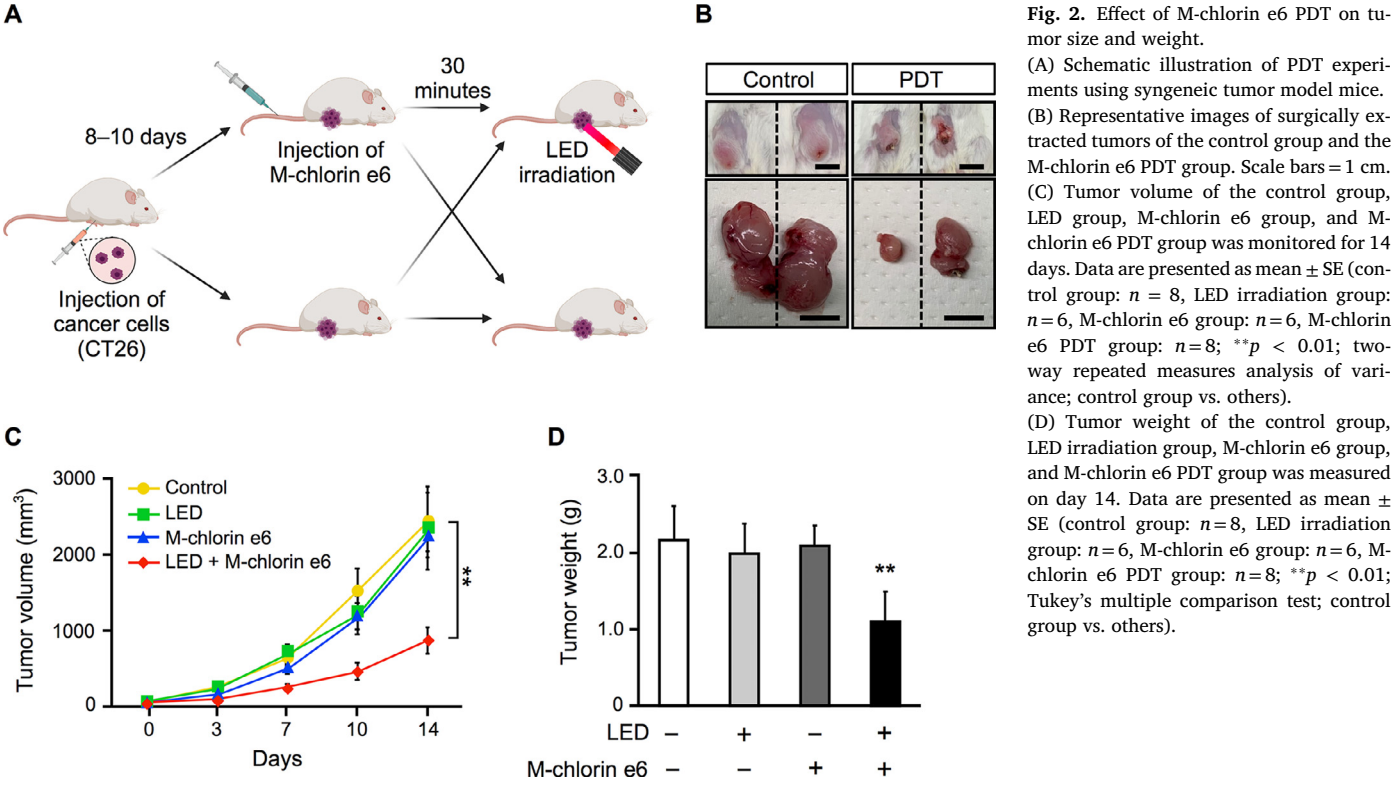

Fig. 2. Effect of M-chlorin e6 PDT on tumor size and weight.
(A) Schematic illustration of PDT experiments using syngeneic tumor model mice.
(B) Representative images of surgically extracted tumors of the control group and the M-chlorin e6 PDT group. Scale bars = 1 cm.
(C) Tumor volume of the control group, LED group, M-chlorin e6 group, and M-chlorin e6 PDT group was monitored for 14 days. Data are presented as mean ± SE (control group: $n = 8$, LED irradiation group: $n = 6$, M-chlorin e6 group: $n = 6$, M-chlorin e6 PDT group: $n = 8$; $^{**}p < 0.01$; two-way repeated measures analysis of variance; control group vs. others).
(D) Tumor weight of the control group, LED irradiation group, M-chlorin e6 group, and M-chlorin e6 PDT group was measured on day 14. Data are presented as mean ± SE (control group: $n = 8$, LED irradiation group: $n = 6$, M-chlorin e6 group: $n = 6$, M-chlorin e6 PDT group: $n = 8$; $^{**}p < 0.01$; Tukey's multiple comparison test; control group vs. others).

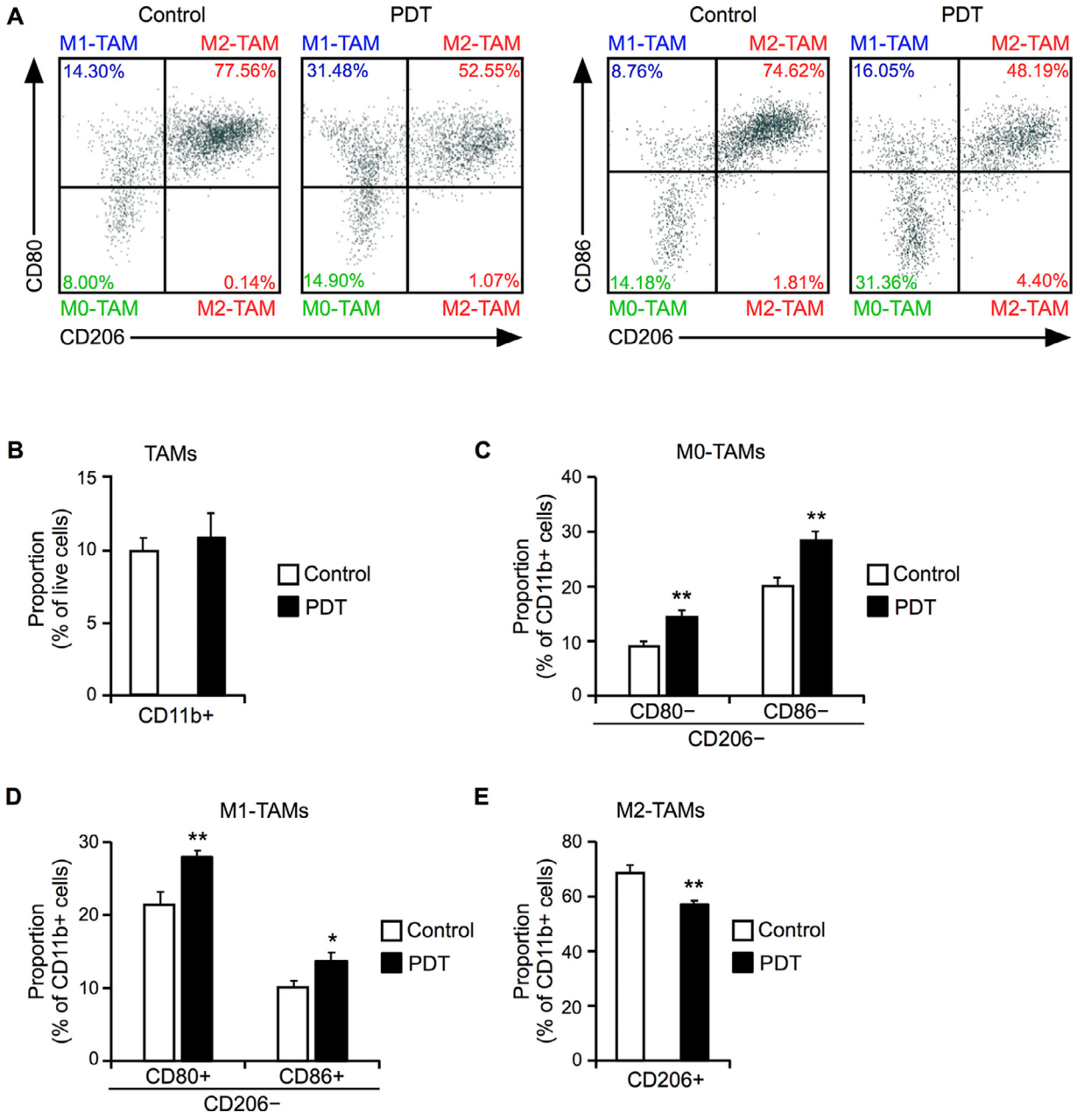

Fig. 3. Effect of M-chlorin e6 PDT on the populations of M1-TAMs and M2-TAMs.
(A) Representative results of flow cytometric analyses on day 2 after LED irradiation. $CD11b^+$, $CD80^-$ or $CD86^-$, $CD206^-$ cells are defined as M0-TAMs. $CD11b^+$, $CD80^+$ or $CD86^+$, $CD206^-$ cells are defined as M1-TAMs. $CD11b^+$, $CD206^+$ cells are defined as M2-TAMs.
(B) Proportion of TAMs ($CD11b^+$ cells) in live cells. Data are presented as mean ± SE ($n = 8$; Student's *t*-test).
(C) Proportion of M0-TAMs ($CD11b^+$, $CD80^-$ or $CD86^-$, $CD206^-$ cells) among all TAMs ($CD11b^+$ cells). Data are presented as mean ± SE ($n = 8$; $^{**}p < 0.01$; Student's *t*-test).
(D) Proportion of M1-TAMs ($CD11b^+$, $CD80^+$ or $CD86^+$, $CD206^-$ cells) among all TAMs ($CD11b^+$ cells). Data are presented as mean ± SE ($n = 8$; $^{*}p < 0.05$, $^{**}p < 0.01$; Student's *t*-test).
(E) Proportion of M2-TAMs ($CD11b^+$, $CD206^+$ cells) among all TAMs ($CD11b^+$ cells). Data are presented as mean ± SE ($n = 8$; $^{**}p < 0.01$; Student's *t*-test).

to the control group (Fig. 3A and D). Importantly, the proportion of M2-TAMs ($CD11b^+$, $CD206^+$) was decreased in the PDT group compared to the control group (Fig. 3A and E). To assess whether the M0-TAMs later polarized into M2-TAMs, flow cytometric analysis was performed on day 7 after LED irradiation and revealed that there was no increase in the number of M2-TAMs compared to the control group (Supplementary Fig. S1). Expression levels of genes encoding M1 markers (iNOS, IL-6, TNF-α, and IL-1β) and M2 markers (arginase, TGF-β, and IL-10) in TAMs ($CD11b^+$) purified using FACSAria were assessed by RT-qPCR. No significant differences in gene expression between the two groups were observed, although expression of the gene encoding the typical M1 marker iNOS tended to increase (Supplementary Fig. S2). The proportions of CTLs and Tregs in the M-chlorin e6 PDT group were equivalent to those of the control group (Supplementary Fig. S3).

M-chlorin e6 also damages cancer cells

We also examined whether PDT using either M-chlorin e6 or G-chlorin e6 directly affects cancer cells using the WST-8 assay (Fig. 4A). M-chlorin e6 PDT reduced the number of CT26 cells, comparable to G-

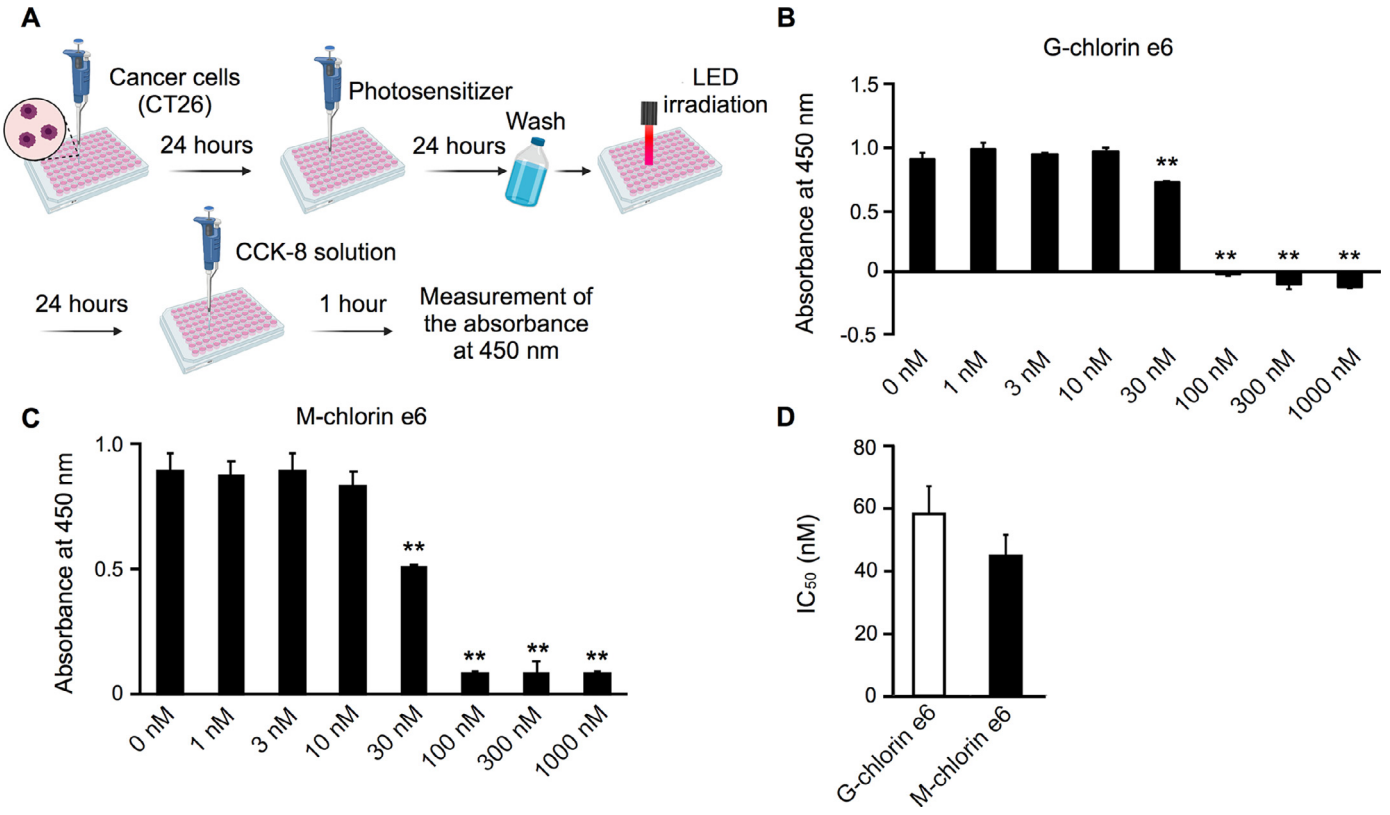

Fig. 4. Effect of M-chlorin e6 PDT on cultured tumor cells.
(A) Schematic illustration of *in vitro* PDT experiments.
(B) Effect of G-chlorin e6 PDT on the viability of CT26 cells. Data are presented as mean ± SE ($n = 5$; $^{**}p < 0.01$; Tukey's multiple comparison test; 0 nM group vs. others).
(C) Effect of M-chlorin e6 PDT on the viability of CT26 cells. Data are presented as mean ± SE ($n = 8$; $^{**}p < 0.01$; Tukey's multiple comparison test; 0 nM group vs. others).
(D) IC_{50} values of treatment with G-chlorin e6 and M-chlorin e6 in combination with LED irradiation. Data are presented as mean ± SE (G-chlorin e6 PDT group: $n = 4$, M-chlorin e6 PDT group: $n = 8$; Student's *t*-test).

chlorin e6 PDT (Fig. 4B and C). The IC_{50} value of M-chlorin e6 was comparable to that of G-chlorin e6 (Fig. 4D). M-chlorin e6 PDT also exhibited cytotoxicity to HCT116 human colon cancer cells (Supplementary Fig. S4). However, M-chlorin e6 treatment without LED irradiation did not exert any cytotoxic effects (Supplementary Fig. S5).

Discussion

It has been reported that the higher the expression of M2 markers in TAMs, the higher the histologic grade and the worse the clinical prognosis [23]. Macrophage migration inhibitors, such as CCR2 inhibitors, have been developed to prevent the accumulation of peripheral blood–derived monocytes, the source of TAMs, in tumor tissues [24]. CCR2 inhibitors have a strong anti-tumor effect when used in combination with anti-tumor drugs, whereas a weak anti-tumor effect is observed with single-agent use. However, the effect of CCR2 inhibitor therapy is not still clear, because migration inhibitors cannot affect resident-tissue macrophages and TAMs that were already present prior to treatment. Furthermore, CCR2 inhibitors non-specifically inhibit TAMs and normal macrophages present throughout the body. In this study, we devised a new photosensitizer for PDT to overcome these problems. We demonstrated that M-chlorin e6, which exhibited rapid excretion and high tissue selectivity, damaged immunosuppressive macrophages, M2-TAMs, in addition to cancer cells. Both M-chlorin e6 and G-chlorin e6 exhibited cancer cell–specific accumulation and were more readily excreted from the body than the second-generation photosensitizer talaporfin sodium. Moreover, M-chlorin e6 PDT significantly reduced tumor volume and weight in syngeneic tumor model mice. Importantly, M-chlorin e6 PDT decreased the proportion of M2-TAMs and increased that of M1-TAMs in the TME. M-chlorin e6 PDT also damaged cultured cancer cells *in vitro*. These results suggest that in addition to its direct anti-cancer cytotoxic effect, M-chlorin e6 stimulates tumor immunity by polarizing TAMs to anti-tumor M1-TAMs. Therefore, it is hypothesized that M-chlorin e6 exerts anti-tumor effects by directly damaging cancer cells and activating anti-tumor immune responses.

The expression levels of genes encoding M1 markers (iNOS, IL-6, TNF-α, and IL-1β) and M2 markers (arginase, TGF-β, and IL-10) in whole TAMs were unchanged. The proportion of M1-TAMs and M2-TAMs among all TAMs changed by only a few tens of percent, which might not have been reflected in gene expression levels. Although M2-TAMs decreased and M1-TAMs increased after PDT, the proportions of CTLs and Tregs did not change. This suggests that the decrease in M2-TAMs induced by PDT has no effect on the rates of CTLs and Tregs. However, the tumor immune function of CTLs and Tregs could be affected, and this possibility needs to be examined in detail in the future. At the very least, a reduction in M2-TAMs would be expected to exert an anti-tumor effect via a reduction in cytokine release, which is necessary for tumor and tumor vessel growth.

In recent years, immune checkpoint inhibition therapy using anti–PD-1/PD-L1 antibodies has been used to treat various solid tumors [23]. Typically, PD-L1 is expressed in cancer cells, whereas PD-1 is expressed in T cells. Recent studies reported that PD-1 and PD-L1 are also expressed in TAMs, which are involved in immunosuppression [25,26]. It has also been reported that the presence of TAMs weakens the thera-

peutic effect of PD-1/PD-L1 inhibitor therapy [27] and that the effect of TAM-targeted therapies is often enhanced when combined with PD-1 inhibitor therapy [28,29]. Taking these findings into account, the combination of M-chlorin e6 PDT and PD-1/PD-L1 inhibitor therapy may provide additional anti-tumor effects. This is a subject for future study.

Monocytes in the bloodstream adhere to vascular endothelial cells and infiltrate into tumor tissues. The infiltrating macrophages, M0-TAMs, can be polarized into M2-TAMs by various cancer cell–derived factors, such as fatty acids and TGF-β [8]. Flow cytometry results showed that the percentage of M0-TAMs ($CD11b^+$, $CD80^-$ or $CD86^-$, $CD206^-$) was increased in the M-chlorin e6 PDT group. These results suggest that M-chlorin e6 PDT may attract monocytes and macrophages to the tumor site. Alternatively, ROS generated by M-chlorin e6 PDT might increase the adhesion of monocytes to vascular endothelial cells [30,31]. The percentage of M2-TAMs did not increase even after 1 week of PDT treatment, suggesting that M0-TAMs generated by PDT treatment do not contribute to cancer malignancy.

There were some limitations to this study. First, it is not clear whether M-chlorin e6 is harmless to the human body. Nano-particle drugs using chlorin e6 have been reported as safe in mouse models [32]. In our experiments, WST8 assay results suggested that M-chlorin e6 is not cytotoxic in the absence of LED irradiation. Therefore, we believe that M-chlorin e6 is likely to be safe for humans. However, more specialized experiments will be required to conclusively demonstrate that M-chlorin is harmless to the human body. Second, we were unable to clarify whether the main mechanism of the antitumor effect of M-chlorin e6 PDT involves direct tumor damage or the enhancement of tumor immunity with a reduction in M2-TAMs. We plan to address these issues in future studies.

Conclusions

We demonstrated that the anti-cancer effect of M-chlorin e6 involves damage to both cancer cells and M2-TAMs. This dual effect significantly suppressed tumor growth in experiments using syngeneic tumor model mice. Considering that M-chlorin e6 has a high tumor accumulation rate and is rapidly excreted from the body, M-chlorin e6 holds tremendous potential as a new therapeutic drug for use in cancer PDT.

Author contributions

Tatsuki Soyama: Data curation, formal analysis, writing – original draft, and approval of the final manuscript.

Akira Sakuragi: Data curation, formal analysis, writing – original draft, and approval of the final manuscript.

Daisuke Oishi: Data curation, formal analysis, and approval of the final manuscript.

Yuka Kimura: Data curation, formal analysis, and approval of the final manuscript.

Hiromasa Aoki: Conceptualization, formal analysis, writing – original draft, funding acquisition, and approval of the final manuscript.

Akihiro Nomoto: Resources, funding acquisition, and approval of the final manuscript.

Shigenobu Yano: Resources, funding acquisition, and approval of the final manuscript.

Hirotada Nishie: Methodology, funding acquisition, and approval of the final manuscript.

Hiromi Kataoka: Conceptualization, methodology, writing – original draft, funding acquisition, and approval of the final manuscript.

Mineyoshi Aoyama: Conceptualization, methodology, writing – original draft, funding acquisition, and approval of the final manuscript.

Declaration of competing interest

The authors have no conflict of interest.

Acknowledgements

We acknowledge the assistance of the Research Equipment Sharing Center at Nagoya City University. All illustrations were created using Biorender.com.

Funding

This work was supported in part by Grants-in-Aid for Scientific Research (KAKEN) from the Japan Society for the Promotion of Science [grant numbers 20K22715, 19H02791, 18K05161, 18K15758, 20K08391, 20K08211].

Supplementary materials

Supplementary material associated with this article can be found, in the online version, at doi:10.1016/j.tranon.2020.101005.

References

[1] J. Wang, D. Li, H. Cang, B. Guo, Crosstalk between cancer and immune cells: role of tumor-associated macrophages in the tumor microenvironment, Cancer Med. 8 (2019) 4709–4721.
[2] E.N. Arwert, A.S. Harney, D. Entenberg, Y. Wang, E. Sahai, J.W. Pollard, J.S. Condeelis, A unidirectional transition from migratory to perivascular macrophage is required for tumor cell intravasation, Cell Rep. 23 (2018) 1239–1248.
[3] L. Lin, Y.-S. Chen, Y.-D. Yao, J.-Q. Chen, J.-N. Chen, S.-Y. Huang, Y.-J. Zeng, H.-R. Yao, S.-H. Zeng, Y.-S. Fu, E.-W. Song, CCL18 from tumor-associated macrophages promotes angiogenesis in breast cancer, Oncotarget 6 (2015) 34758–34773.
[4] R. Geiger, J.C. Rieckmann, T. Wolf, C. Basso, Y. Feng, T. Fuhrer, M. Kogadeeva, P. Picotti, F. Meissner, M. Mann, N. Zamboni, F. Sallusto, A. Lanzavecchia, L-Arginine modulates T cell metabolism and enhances survival and anti-tumor activity, Cell. 167 (2016) 829–842 e13.
[5] P. Jeannin, L. Paolini, C. Adam, Y. Delneste, The roles of CSFs on the functional polarization of tumor-associated macrophages, FEBS J. 285 (2018) 680–699.
[6] Y.-L. Zhao, P.-X. Tian, F. Han, J. Zheng, X.-X. Xia, W.-J. Xue, X.-M. Ding, C.-G. Ding, Comparison of the characteristics of macrophages derived from murine spleen, peritoneal cavity, and bone marrow, J. Zhejiang Univ. Sci. B 18 (2017) 1055–1063.
[7] Y. Chen, Y. Song, W. Du, L. Gong, H. Chang, Z. Zou, Tumor-associated macrophages: an accomplice in solid tumor progression, J. Biomed. Sci. 26 (2019) 78.
[8] F. Zhang, H. Wang, X. Wang, G. Jiang, H. Liu, G. Zhang, H. Wang, R. Fang, X. Bu, S. Cai, J. Du, TGF-β induces M2-like macrophage polarization via SNAIL-mediated suppression of a pro-inflammatory phenotype, Oncotarget 7 (2016) 52294–52306.
[9] Y. Lu, L. Guo, G. Ding, PD1+ tumor associated macrophages predict poor prognosis of locally advanced esophageal squamous cell carcinoma, Future Oncol. 15 (2019) 4019–4030.
[10] M. Yang, Z. Li, M. Ren, S. Li, L. Zhang, X. Zhang, F. Liu, Stromal infiltration of tumor-associated macrophages conferring poor prognosis of patients with basal-like breast carcinoma, J. Cancer 9 (2018) 2308–2316.
[11] C. Ngambenjawong, H.H. Gustafson, S.H. Pun, Progress in tumor-associated macrophage (TAM)-targeted therapeutics, Adv. Drug Deliv. Rev. 114 (2017) 206–221.
[12] A. Sica, A. Mantovani, Macrophage plasticity and polarization: in vivo veritas, J. Clin. Investig. 122 (2012) 787–795.
[13] G. Solinas, G. Germano, A. Mantovani, P. Allavena, Tumor-associated macrophages (TAM) as major players of the cancer-related inflammation, J. Leukoc. Biol. 86 (2009) 1065–1073.
[14] A.B. Ormond, H.S. Freeman, Dye sensitizers for photodynamic therapy, Materials 6 (2013) 817–840.
[15] Y. Muragaki, J. Akimoto, T. Maruyama, H. Iseki, S. Ikuta, M. Nitta, K. Maebayashi, T. Saito, Y. Okada, S. Kaneko, A. Matsumura, T. Kuroiwa, K. Karasawa, Y. Nakazato, T. Kayama, Phase II clinical study on intraoperative photodynamic therapy with talaporfin sodium and semiconductor laser in patients with malignant brain tumors, J. Neurosurg. 119 (2013) 845–852.
[16] R. Baskaran, J. Lee, S.-G. Yang, Clinical development of photodynamic agents and therapeutic applications, Biomater. Res. 22 (2018) 25.
[17] H. Nishie, H. Kataoka, S. Yano, H. Yamaguchi, A. Nomoto, M. Tanaka, A. Kato, T. Shimura, T. Mizoshita, E. Kubota, S. Tanida, T. Joh, Excellent anti-tumor effects for gastrointestinal cancers using photodynamic therapy with a novel glucose conjugated chlorin e6, Biochem. Biophys. Res. Commun. 496 (2018) 1204–1209.
[18] T. Osaki, S. Hibino, I. Yokoe, H. Yamaguchi, A. Nomoto, S. Yano, Y. Mikata, M. Tanaka, H. Kataoka, Y. Okamoto, A basic study of photodynamic therapy with glucose-conjugated chlorin e6 using mammary carcinoma xenografts, Cancers 11 (2019) 636.
[19] C. Bensoussan, N. Rival, G. Hanquet, F. Colobert, S. Reymond, J. Cossy, Iron-catalyzed cross-coupling between C-bromo mannopyranoside derivatives and a vinyl Grignard reagent: toward the synthesis of the C31–C52 fragment of amphidinol 3, Tetrahedron 69 (2013) 7759–7770.

[20] P. Shu, J. Zeng, J. Tao, Y. Zhao, G. Yao, Q. Wan, Selective S-deacetylation inspired by native chemical ligation: practical syntheses of glycosyl thiols and drug mercapto-analogues, Green Chem. 17 (2015) 2545–2551.
[21] J.A. Hargus, F.R. Fronczek, G.H. Vicente, K.M. Smith, Mono-(L)-aspartylchlorin-e6, Photochem. Photobiol. 83 (2007) 1006–1015.
[22] Y. Kanda, Investigation of the freely available easy-to-use software "EZR" for medical statistics, Bone Marrow Transpl. 48 (2013) 452–458.
[23] Y. Han, D. Liu, L. Li, PD-1/PD-L1 pathway: current researches in cancer, Am. J. Cancer Res. 10 (2020) 727–742.
[24] T.M. Nywening, A. Wang-Gillam, D.E. Sanford, B.A. Belt, R.Z. Panni, B.M. Cusworth, A.T. Toriola, R.K. Nieman, L.A. Worley, M. Yano, K.J. Fowler, A.C. Lockhart, R. Suresh, B.R. Tan, K.-H. Lim, R.C. Fields, S.M. Strasberg, W.G. Hawkins, D.G. DeNardo, S.P. Goedegebuure, D.C. Linehan, Targeting tumour-associated macrophages with CCR2 inhibition in combination with FOLFIRINOX in patients with borderline resectable and locally advanced pancreatic cancer: a single-centre, open-label, dose-finding, non-randomised, phase 1b trial, Lancet Oncol. 17 (2016) 651–662.
[25] G.P. Hartley, L. Chow, D.T. Ammons, W.H. Wheat, S.W. Dow, Programmed cell death ligand 1 (PD-L1) signaling regulates macrophage proliferation and activation, Cancer Immunol. Res. 6 (2018) 1260–1273.
[26] S.R. Gordon, R.L. Maute, B.W. Dulken, G. Hutter, B.M. George, M.N. McCracken, R. Gupta, J.M. Tsai, R. Sinha, D. Corey, A.M. Ring, A.J. Connolly, I.L. Weissman, PD-1 expression by tumour-associated macrophages inhibits phagocytosis and tumour immunity, Nature 545 (2017) 495–499.
[27] S.P. Arlauckas, C.S. Garris, R.H. Kohler, M. Kitaoka, M.F. Cuccarese, K.S. Yang, M.A. Miller, J.C. Carlson, G.J. Freeman, R.M. Anthony, R. Weissleder, M.J. Pittet, In vivo imaging reveals a tumor-associated macrophage-mediated resistance pathway in anti-PD-1 therapy, Sci. Transl. Med. 9 (2017) eaal3604.
[28] Y. Zhu, B.L. Knolhoff, M.A. Meyer, T.M. Nywening, B.L. West, J. Luo, A. Wang-Gillam, S.P. Goedegebuure, D.C. Linehan, D.G. DeNardo, CSF1/CSF1R blockade reprograms tumor-infiltrating macrophages and improves response to T–cell checkpoint immunotherapy in pancreatic cancer models, Cancer Res. 74 (2014) 5057–5069.
[29] H. Tsukamoto, K. Fujieda, A. Miyashita, S. Fukushima, T. Ikeda, Y. Kubo, S. Senju, H. Ihn, Y. Nishimura, H. Oshiumi, Combined blockade of IL6 and PD-1/PD-L1 signaling abrogates mutual regulation of their immunosuppressive effects in the tumor microenvironment, Cancer Res. 78 (2018) 5011–5022.
[30] L.J. Park, S.M. Ju, H.Y. Song, J.A. Lee, M.Y. Yang, Y.H. Kang, H.J. Kwon, T.-Y. Kim, S.Y. Choi, J. Park, The enhanced monocyte adhesiveness after UVB exposure requires ROS and NF-kappaB signaling in human keratinocyte, J. Biochem. Mol. Biol. 39 (2006) 618–625.
[31] Y.-T. Lin, L.-K. Chen, D.-Y. Jian, T.-C. Hsu, W.-C. Huang, T.-T. Kuan, S.-Y. Wu, C.-F. Kwok, L.-T. Ho, C.-C. Juan, Visfatin promotes monocyte adhesion by up-regulating ICAM-1 and VCAM-1 expression in endothelial cells via activation of p38-PI3K-Akt signaling and subsequent ROS production and IKK/NF-κB activation, Cell. Physiol. Biochem. 52 (2019) 1398–1411.
[32] Rational design of oxygen deficient TiO2−x nanoparticles conjugated with chlorin e6 (Ce6) for photoacoustic imaging-guided photothermal/photodynamic dual therapy of cancer, Nanoscale 12 (2020) 1707–1718.